J. Fluid Mech. (2002), *vol.* 459, *pp.* 217–243.
DOI: 10.1017/S0022112002007954 Printed in the United Kingdom

Turbulence mechanism in Klebanoff transition: a quantitative comparison of experiment and direct numerical simulation

By S. BAKE[1], D. G. W. MEYER[2] AND U. RIST[2]

[1]Hermann-Föttinger-Institut für Strömungsmechanik, Technische Universität Berlin, Straße des 17. Juni 135, 10623 Berlin, Germany

[2]Universität Stuttgart, Institut für Aerodynamik und Gasdynamik, Pfaffenwaldring 21, 70550 Stuttgart, Germany

(Received 26 October 2000 and in revised form 14 November 2001)

The mechanism of turbulence development in periodic Klebanoff transition in a boundary layer has been studied experimentally and in a direct numerical simulation (DNS) with controlled disturbance excitation. In order to compare the results quantitatively, the flow parameters were matched in both methods, thus providing complementary data with which the origin of turbulence in the transition process could be explained. Good agreement was found for the development of the amplitude and shape of typical disturbance structures, the Λ-vortices, including the development of ring-like vortices and spikes in the time traces. The origin and the spatial development of random velocity perturbations were measured in the experiment, and are shown together with the evolution of local high-shear layers. Since the DNS is capable of providing the complete velocity and vorticity fields, further conclusions are drawn based on the numerical data. The mechanisms involved in the flow randomization process are presented in detail. It is shown how the random perturbations which initially develop at the spike-positions in the outer part of the boundary layer influence the flow randomization process close to the wall. As an additional effect, the interaction of vortical structures and high-shear layers of different disturbance periods was found to be responsible for accelerating the transition to a fully developed turbulent flow. These interactions lead to a rapid intensification of a high-shear layer very close to the wall that quickly breaks down because of the modulation it experiences through interactions with vortex structures from the outer part of the boundary layer. The final breakdown process will be shown to be dominated by locally appearing vortical structures and shear layers.

1. Introduction

1.1. *General description of the problem*

The laminar–turbulent transition process in shear layers has been investigated for more than a century, and many different concepts for the explanation of the mechanisms involved have been developed. In wall-bounded shear layers the type of transition depends strongly on the character of the external perturbations. As a first approach, two different classes of transition can be distinguished. The first class exhibits growth of low-amplitude boundary-layer disturbances according to linear stability theory, followed by nonlinear interactions of waves and vortices, eventually leading to a breakdown to turbulence. In the second class, the initial disturbance

amplitudes are large enough to initiate 'bypass-transition', a term introduced by Morkovin (1969). This paper is devoted to a combined experimental and numerical study of a type of transition belonging to the first class, the Klebanoff regime. The Klebanoff regime of transition was chosen because of its comparability with previous studies, and because of the similar characteristics found in other regimes. Very similar vortex structures develop from the instability waves in other transition types, i.e. in the N-regime (Bake, Fernholz & Kachanov 2000) and the oblique transition (Berlin, Weigel & Henningson 1999), possibly indicating a universal local transition mechanism.

1.2. *The Klebanoff regime*

The Klebanoff regime, or K-regime, has been studied in many experimental investigations beginning with Hama (1959) who was the first to observe the importance of vortex loops and their induction at the late stages of transition. The generation of turbulence was observed by Hama above the 'legs' and at the upstream part of the vortex loop. A more detailed investigation of the shape and the characteristics of the Λ-vortex was performed by Kovasznay, Komoda & Vasudeva (1962). Their contour plots of the vorticity distribution were reproduced numerically much later with remarkable similarity by Wray & Hussaini (1984). However, the position of the 'spikes' was not determined correctly by Kovasznay *et al.* (1962), and it was not clear whether they could be identified as the first cells of the developing turbulence. Hama & Nutant (1963) visualized the development of the Λ-vortex by means of the hydrogen-bubble technique, and these figures were later computed again by Zang & Hussaini (1987). The resemblance of the two was shown by Kleiser & Zang (1991). Two important properties of these structures had already been found by Hama & Nutant (1963): during the roll-up of the tip of the Λ-vortex, an Ω-shaped vortex (the hairpin vortex of Klebanoff) develops which then detaches and reconnects to a ring-like vortex. This roll-up, detachment and reconnection was observed up to four or five times in a cascade. Furthermore, a strong shear layer with a Δ-wing shape was induced by the vortex legs on the back of the Λ-vortex and eventually broke down.

In the famous experiment of Klebanoff, Tidstrom & Sargent (1962), a vibrating ribbon – a device that has been in use in transition experiments since Schubauer & Skramstad (1947) – was used in combination with spanwise periodic spacers to excite two- and three-dimensional waves under controlled conditions in the boundary layer. With this work, it became clear that the non linear interaction of waves is a strong driving force behind the transition to turbulence. They observed the formation of 'peak' planes (strong fluctuations) and 'valley' planes (weak fluctuations) resulting in a spanwise modulation of the wavefronts. Vortex structures developed from this modulation, and the maxima of the fluctuations in the 'peak' planes grew rapidly, leading to the breakdown to turbulence. So-called 'spikes' (high-frequency, flash-like oscilloscope traces) appeared in the 'peak' planes, doubling and multiplying further downstream. At first, these 'spikes' were interpreted as secondary instabilities. This interpretation was apparently incorrect, since the 'spikes' are the result of the induced negative velocity at the centre of ring-like vortices at the tip of a Λ-shaped vortex structure, as found by Borodulin & Kachanov (1989). Experimental results (Borodulin & Kachanov 1995), as well as numerical simulations (Rist 1990; Rist & Fasel 1995; Rist & Kachanov 1995), of flat-plate boundary-layer flows have shown that the 'spikes' can be found exactly in the centre of the ring-like vortices and are not a result of a secondary shear-layer instability.

A very similar sequence of events was found experimentally by Nishioka and

co-workers for the case of plane Poiseuille flow (see e.g. Nishioka, Asai & Iida (1980, 1981) and Nishioka & Asai 1984). They also found initial growth of the Tollmien–Schlichting waves in accordance with linear stability theory, and in later stages, the typical peak–valley splitting, the formation of characteristic Λ-vortices and concomitant high-shear layers, as well as the occurrence of spike signals prior to the very fast final stages of the breakdown process to a turbulent flow. The first signs of flow randomization were initially observed in the vicinity of the spike signals, as in the flat-plate boundary-layer case studied here.

The behaviour of the vortical structures due to self-induction was first investigated by Hama & Nutant (1961). Later, Moin, Leonard & Kim (1986) investigated the development of a hairpin vortex by means of Biot–Savart calculations, and computed the evolution of a vortex layer using the Navier–Stokes equations. Both methods show that a ring-like vortex detaches by self-induction of the vortices and generates a region of high Reynolds stresses. This behaviour exhibits a strong similarity with the 'typical eddies' shown by Falco (1977) by means of smoke visualization in the outer region of a turbulent boundary layer.

The hypothesis of Theodorsen (1952), stating that the hairpin or horseshoe vortices play a key role in the production process of turbulence, has motivated many researchers to investigate these structures in detail. Some, like Head & Bandyopadhyay (1981), tried to find them directly in the turbulent boundary layer. Others, like Acalar & Smith (1987*a*, *b*) and Haidari & Smith (1994), investigated artificially excited hairpin vortices (by local injection or half-spheres). The latter showed that a single hairpin vortex can decay without producing turbulence. But in the case where a hairpin vortex stimulates the generation of secondary vortices, the whole structure grows and spreads in the boundary layer.

Under controlled disturbance conditions, the flow in this regime remains deterministic (periodic) until a rather late stage of the transition process. The present knowledge about the transition process in the K-regime can be summarized as follows (for an extended overview see Kachanov 1994):

(*a*) growth of the three-dimensional instability modes at the fundamental ($f = f_1$) and zero frequencies (mean flow deformation);

(*b*) formation of periodic streamwise vortices and growth of a spanwise modulation of the mean velocity and the disturbance amplitudes (and phases) leading to the formation of 'peaks' and 'valleys' in the spanwise distributions, with very high amplitudes of the perturbations at the peak positions;

(*c*) formation of Λ-structures (at each period of the fundamental wave) aligned in rows consisting mainly of a continuously deforming vortex loop (Λ-vortex) and a three-dimensional (Δ- or Λ-shaped) high-shear layer;

(*d*) continuous stretching of the Λ-structures and concentration of the vorticity in the 'legs' of the Λ-vortices and in the high-shear layers that occur together with these vortices in the boundary layer;

(*e*) rapid (but not explosive) growth of the 3-D high-frequency spectral modes;

(*f*) multiple reconnection of the Λ-vortex 'legs' near the tip and formation of ring-like vortices (through an intermediate stage of the Ω-vortices, also known as hairpin vortices);

(*g*) appearance of very intensive flashes in the streamwise-velocity time traces at the centre of the ring-like vortices, called 'spikes', which occur in increasing number in downstream direction;

(*h*) growth of quasi-random, non-periodic perturbations observed in the near-wall region in the vicinity of the peak position.

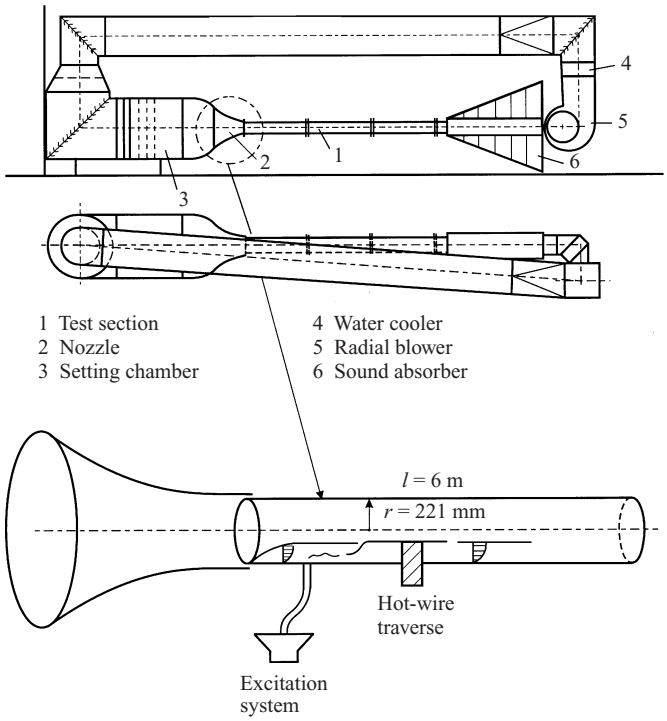

FIGURE 1. The laminar wind tunnel at the HFI.

The early stages of the transition process, including the stages of wave growth according to primary and secondary instability theory, as well as the initial formation of the Λ-structures, are basically understood. The late stages of the transition process which we study here, as represented by (*e*)–(*h*) in the list given above, are not quite so well understood as the earlier ones. In particular, the mechanism of flow randomization, and the final breakdown of the vortex structures in this scenario, have not been fully explained yet. One of the goals of the present work is to shed some light on this problem. New details of the development of random perturbations in the three-dimensional vortex structures of the K-regime will be presented. The experimental results in the K-regime will be compared in detail with a DNS which was specifically set up to reproduce the experimental mean flow and disturbance excitation conditions as closely as possible.

2. Experimental methods

2.1. *Wind tunnel*

The experiments were performed in the laminar wind tunnel of the Hermann-Föttinger-Institute of the Berlin Technical University (figure 1). It is a closed-circuit tunnel with an axisymmetric test section made of Plexiglas tubes of various lengths with an inner diameter of 0.44 m and a total length of 6 m. It has a centrifugal fan and an additional blower to blow out the nozzle boundary layer at the entry of the test section. In order to reduce the noise level in the wind tunnel, various sound attenuation devices are installed. In the settling chamber, a non-woven filter mat and a single, precisely manufactured, perforated metal plate (64% open area ratio) are inserted to reduce mean flow non-uniformities. The settling chamber is followed by a

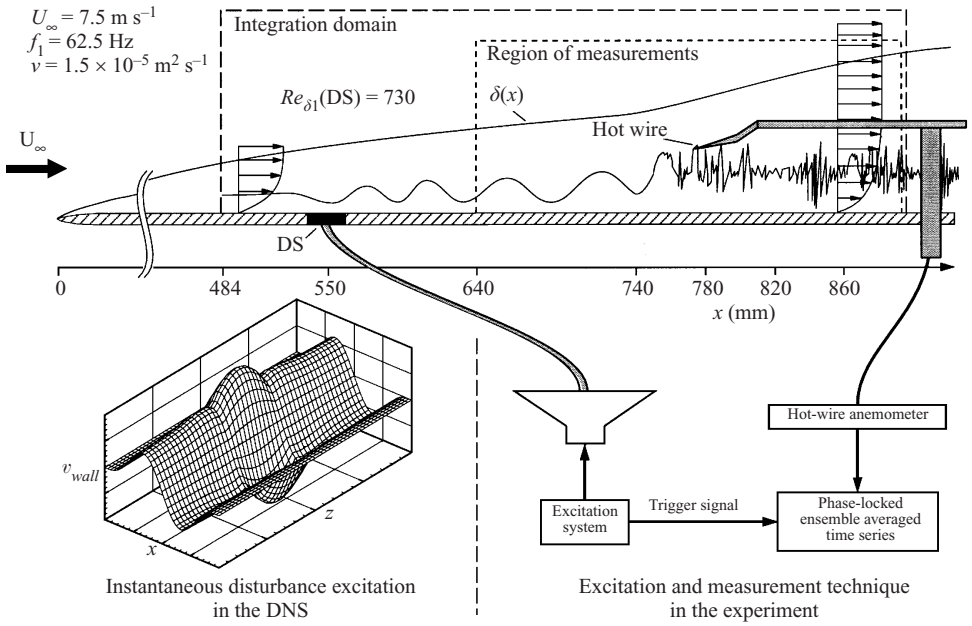

FIGURE 2. Sketch of the integration domain, the measurement region, and the excitation system in the experiment and the DNS.

2 m long axisymmetric nozzle with an 18 : 1 contraction ratio. The free-stream turbulence level was $Tu_\infty = 0.04\%$ in the frequency range between 0.1 and 1000 Hz at a free-stream velocity $U_\infty = 7.5\,\mathrm{m\,s^{-1}}$. In the laminar boundary layer, a maximum level of around $u'/U_\infty = 0.12\%$ was found within a profile typical of the Klebanoff mode. The main content of disturbances was found in the spectrum below 5 Hz, resulting from low-frequency volume fluctuations in the wind tunnel. The flow temperature can be controlled with a water cooler to within $\pm 0.05\,^\circ$C. For a further description of the flow quality, see Fernholz & Warnack (1998).

The boundary layer under investigation starts at the elliptic leading edge of the axisymmetric test section of the wind tunnel and develops downstream on its inner wall. Because of the axisymmetric shape of the test section, no corner-flow effects can occur. Spanwise curvature effects were neglected because the ratio of the boundary-layer thickness $\delta_{99\%}$ at the position of the excitation source to the radius of the test-section r was about 0.03. The coordinate system is defined with x in the streamwise direction starting at the leading edge, y is the wall-normal distance, and z is the spanwise direction along the circumference of the wall of the test section, and is defined as zero on the symmetry line of the excited disturbance at the position of the excitation source.

2.2. *Methods of measurement*

All measurements in the flow were conducted with a constant-temperature hot-wire anemometer (AA-Lab AN-1003). The streamwise velocity component was measured with a gold-plated tungsten/platinum hot wire with a diameter of 2.5 μm and an effective length of 0.55 mm. It was mounted on an electrically driven xy-traverse and was calibrated against a Prandtl tube in the free stream.

A sketch of the disturbance excitation and the data acquisition system is shown in figure 2. The hot-wire signal was sampled together with a trigger signal generated by

the excitation system. The sample rate was chosen to obtain at least 64 samples in each period of a wave with the fundamental excitation frequency of $f_1 = 62.5$ Hz. A typical measurement in a (y, z)-plane with a grid of $n_y \times n_z = 38 \times 23 = 876$ points took three hours of total measuring time.

After the transfer of the data to a work-station, the trigger signal was extracted from the time series and the data were processed to obtain the statistics and the phase-locked ensemble averaged time series. The trigger signal was a short square-wave impulse generated with half the fundamental, i.e. the subharmonic frequency. It allowed us to split the measured signal into its periodic and non-periodic parts.

Klebanoff excited transition with a vibrating ribbon. In order to control the desired spanwise periodicity, he placed spacers of scotch tape on the wall below the ribbon. The disadvantage of this method is that a slight difference in position and height of the tape causes significant changes in the flow, and many test measurements are necessary to obtain the desired result (amplitude, symmetry). With a slit source connected to loudspeakers, the frequency, amplitude, phase and spanwise wavenumber of the excited wave can be varied continuously, by feeding different signals to the loudspeakers. In the present case, the source excited a quasi-two-dimensional harmonic instability wave with the frequency $f_1 = 62.5$ Hz ($F_1 = 2\pi f_1 \nu / U_\infty^2 = 105 \times 10^{-6}$ with the kinematic viscosity $\nu = 1.5 \times 10^{-5}\,\mathrm{m^2\,s^{-1}}$) that had a spanwise modulation of its amplitude and phase. This leads to the well-known Klebanoff regime characterized by a spanwise-modulated high-amplitude fundamental wave followed by the formation of a peak and valley structure, aligned Λ-vortices, and typical 'spikes' appearing in the oscilloscope traces.

The excitation signals were generated by a PC, fed into a 16 channel DA-converter and led to an array of calibrated power amplifiers. The instability waves were introduced into the boundary layer by means of a spanwise slit with a width of 0.8 mm, a length of 260 mm (19% of total circumference (1387 mm) of the test section) and a depth of 5.0 mm. The slit was cut into the wall of a special ring-like part of the test section. A set of 32 specially shaped metal pipes (with a spacing of 8 mm each) was positioned along the slit. Outside the wind tunnel the pipes were connected to the loudspeakers by an array of plastic tubes. The ring with the slit generator was inserted between two other segments of the test section and could be rotated in order to change the spanwise position of the source relative to the hot-wire probe mounted on an xy-traverse. Inside the slit source, the signals were produced by the different loudspeakers and superimposed in the flow near the outlet to form a two- or three-dimensional disturbance field of volume fluctuations of the fluid.

The trigger signal, recorded together with the hot-wire data, enabled us to split the total velocity into the mean velocity $\bar{u}$, the ensemble-averaged periodically fluctuating velocity u'_p and the (random) deviation u'_r from the average periodic signal according to

$$U(x, y, z, t) = \bar{u}(x, y, z) + u'_p(x, y, z, t) + u'_r(x, y, z, t), \tag{2.1}$$

where

$$\bar{u}(x, y, z) = \frac{1}{N} \sum_{i=1}^{N} U(x, y, z, t_i), \quad t_i = (i-1)\Delta t \tag{2.2}$$

and

$$u'_p(x, y, z, t) = \frac{1}{NP} \sum_{k=1}^{NP} u'(x, y, z, t_k), \quad t_k = (k-1)T + t \tag{2.3}$$

(N: total number of samples for all periods, NP: total number of periods, Δt: sam-

pling interval, T: time of one fundamental period). Here, U is the total velocity and u' the total disturbance with respect to the time-averaged flow $\bar{u}$, and u'_r is the random part of the perturbation, defined as the deviation of the instantaneous time signal from the periodic part of the flow $\bar{u} + u'_p$, computed according to (2.1). It can be averaged again for each phase angle of the excited disturbance in order to calculate an r.m.s.-value. It cannot be separated into spatial and temporal fluctuations because the measurements were performed with a single hot wire. However, it can be regarded as a measure of the development of stochastic turbulence in the transition process.

The Fourier coefficients of the velocity fluctuations at a fixed x-position are computed using the periodic ensemble-averaged part of the velocity fluctuation only:

$$A_h(y,z) = \sum_{h=1}^{h_{max}} u'_p(y,z,\tau)\mathrm{e}^{-\mathrm{i}h\omega\tau}, \tag{2.4}$$

with h being the frequency index, and $h = 1$ denoting the fundamental frequency.

The procedure for decomposing a spatial wave packet into a fan of three-dimensional oblique waves in the experiment was similar to that used by Gilyov, Kachanov & Kozlov (1983), and is described in more detail by Kachanov & Michalke (1994). After the temporal Fourier transformation of the periodic velocity fluctuations u'_p the spanwise wavenumber spectra $B_{h,k}$ were calculated using

$$B_{h,k}(y) = \sum_{k=0}^{k_{max}} U_p(y,z)\mathrm{e}^{-\mathrm{i}k\gamma z} \quad \text{for} \quad h = 0, \tag{2.5}$$

describing the stationary disturbances, with U_p being the mean flow deformation, and k being the spanwise wavenumber index. For the unsteady disturbances,

$$B_{h,k}(y) = \sum_{k=0}^{k_{max}} A_h(y,z)\mathrm{e}^{-\mathrm{i}k\gamma z} \quad \text{for} \quad h = 1,2,3,\ldots \tag{2.6}$$

is used with $\gamma = 2\pi/\lambda_z$ being the spanwise wavenumber (λ_z is given by the width of the domain in the spanwise direction).

3. Numerical methods

The details of the DNS method used here, along with its continuing development, have been described in Fasel, Rist & Konzelmann (1990), Kloker, Konzelmann & Fasel (1993), Rist & Fasel (1995) and Kloker (1998). Therefore, only a short overview will be given.

The numerical method is based on a velocity–vorticity formulation of the Navier–Stokes equations for an incompressible fluid. The so-called spatial model is applied, where all three spatial dimensions and time are discretized without any modelling assumptions. For the present simulation, the flow is split into a steady two-dimensional baseflow and an unsteady three-dimensional disturbance flow. The baseflow has to be calculated separately before the equations for the disturbance flow field can be solved. In this model the nonlinear baseflow deformation is obtained as the temporal mean of the fluctuating disturbance quantities at any given point in the flow field.

Since the flow is considered to be periodic in the spanwise direction, a Fourier ansatz in this direction is used, and the equations and boundary conditions are transformed accordingly. The nonlinear terms are solved using a pseudo-spectral technique introduced by Orszag (1971) which ensures an aliasing-free computation of all spanwise modes.

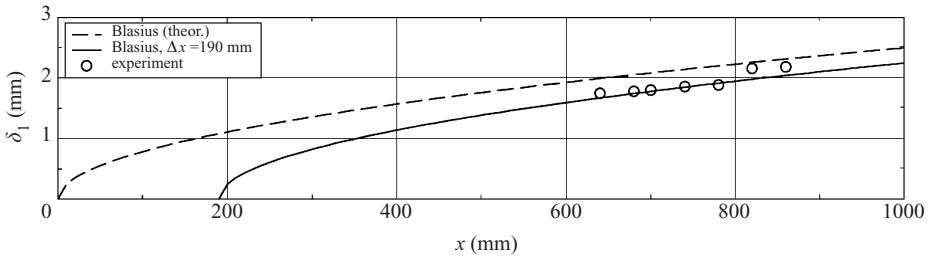

FIGURE 3. Development of the displacement thickness δ_1 in comparison with the theoretical Blasius curve, and with the Blasius curve shifted by $\Delta x = 190$ mm.

High-order compact finite differences are used for discretization of the wall-normal and the downstream direction on an equidistant grid. At the wall, a zone with a refined mesh (half the step size in the wall-normal direction) is used in order to ensure sufficient resolution for the dynamics of the flow close to the wall at the very late stages of the transition process (see figure 6 at $x = 860$ mm). Explicit time integration is performed by a standard Runge–Kutta scheme of fourth-order accuracy. A scheme of alternating high-order up- and downwind compact finite differences is used in subsequent Runge–Kutta substeps for computation of the derivatives of the nonlinear terms. This method leads to a finite difference scheme with essentially the characteristics of a central scheme, but, in addition, provides the right amount of numerical damping (small enough to allow for the correct computation of the instabilities involved but also large enough to stabilize the numerical method).

The disturbances in the DNS are generated by suction and blowing within a disturbance strip at the wall (see figure 2). The wall-normal velocity component is defined by

$$v_{wall}(x, z) = [A_{2-D} + A_{3-D}\, f(z)]\, g(x) \sin(\omega t), \tag{3.1}$$

where A_{2-D} and A_{3-D} are the disturbance amplitudes, with $g(x)$ and $f(z)$ being functions which assure zero net mass flux into the integration domain at any time. Additionally, $f(z)$ represents the wave modulation in the spanwise direction and is chosen to create an initial disturbance spectrum in the spanwise direction that is as close to the experiment as possible.

In a buffer domain at the outflow boundary, the disturbance vorticity vector is forced to zero over a short range in the downstream direction. This damping process does not lead to any significant upstream influence either in the vorticity or the velocity field. The vanishing vorticity leads to an exponential decay of all velocity components. At the end of the buffer domain, the velocity disturbances are reduced by several orders of magnitude. The details of the implementation of the outflow boundary condition are only of minor relevance in this case.

The method has been extensively verified (checked for consistent discretization and convergence) and validated (compared with linear stability theory and experimental data) and has proven to be a useful research tool. For further details, the reader is referred to the references given above.

4. Matching of DNS and experiment

A sketch of the setup of the boundary-layer flow studied showing the numerical integration domain and the measurement region is given in figure 2. All downstream

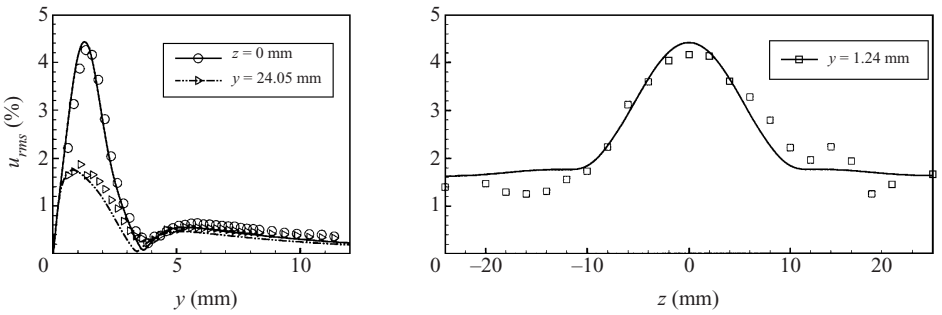

FIGURE 4. Initial conditions for the K-regime. Wall-normal and spanwise amplitude profiles at $x = 640$ mm for the fundamental frequency. Experiment (symbols) vs. DNS (lines).

positions are given in experimental coordinates, as a convenient scaling is not available over the full range of the transition process from laminar to turbulent flow. The virtual leading edge of the undisturbed Blasius baseflow is located at $\Delta x = 190$ mm downstream of the physical leading edge of the channel (figure 3). The disturbance strip is located at $Re_{\delta 1} = 730$, which corresponds to a position of $x = 550$ mm relative to the physical leading edge. The positions chosen for comparison of the results are also given in figure 2.

The amplitudes of the Tollmien–Schlichting (TS) waves had to be quite large from the very beginning in order to trigger the transition within a short distance downstream of the disturbance source and to reach at least a four-spike stage within the measurement region. Therefore, nonlinear wave interactions are already important at the first data acquisition point in the experiment. Since this point at $x = 640$ mm is located about two TS-wavelengths ($\lambda_{TS} \approx 43$ mm, $\alpha_{TS} \approx 0.146\,\text{mm}^{-1}$) downstream of the disturbance source, iterative adjustments of the disturbance amplitudes at the disturbance strip in the DNS were necessary in order to obtain good overall agreement with the experiment – not only for the u_{rms}-profiles in the wall-normal and spanwise directions at the first measurement position (see figure 4), but also for the development of the disturbance amplitudes over the whole transition process (see figure 8). Figure 4 also shows the relative amplitudes of the two-dimensional wave and the spanwise modulation 90 mm downstream of the disturbance source, i.e. we have approximately a two-dimensional TS-wave of 1.5%, and a three-dimensional modulation that leads to a total amplitude of about 4.5% for the fundamental frequency at the first measurement position.

When exciting the Klebanoff regime, the question arises of how to choose the spanwise periodicity of the peak positions. A direct numerical simulation of Meyer, Rist & Wagner (1998) showed that increasing the spanwise spacing of the vortices delays transition slightly. However, the qualitative nature of the transition process close to the peak plane, including the formation of Λ-vortices, high-shear layers, and their subsequent breakdown, remains unchanged. In early experiments the problem occurred that an overlap of spanwise-distributed vortical structures made it difficult to distinguish the production process of higher-order structures and their breakdown to turbulence. Therefore, a spanwise spacing of the peak-positions of $\lambda_{z\,EXP} = 96$ mm ($\gamma_{EXP} = 0.065\,\text{mm}^{-1}$) has been chosen where the Λ-vortices did not interact within the measurement region. Only the central peak position is considered in the further description of the results. In the DNS a spanwise period of $\lambda_{z\,DNS} = 80$ mm ($\gamma_{DNS} =$

Size of the integration domain in mm ($\Delta X \times \Delta Y \times \Delta Z$)	$541.53 \times 18.48 \times 80.00$
Number of grid points ($n_x \times n_y$)	2266×361
Number of Fourier modes (de-aliased)	154
Total number of unknowns	$\approx 125 \times 10^6$
Number of grid points per wavelength in spanwise direction (for computation of the nonlinear terms)	512
Number of grid points within the wall-zone	33
Numerical resolution in mm ($\Delta x \times \Delta y$ (wall-zone) $\times \Delta z$)	$0.2391 \times 0.0537(0.0269) \times 0.2614$
Numerical resolution in wall units at $x = 900$ mm ($\Delta x^+ \times \Delta y^+ \times \Delta z^+$)	$\approx 7.2 \times 0.8 \times 7.8$
Numerical time step Δt (s)	1.067×10^{-5}
Number of disturbed Fourier modes	21

TABLE 1. Parameters of the simulation.

$0.078\,\mathrm{mm}^{-1}$) was found to be sufficient to separate the adjacent Λ-vortices without any significant interaction inside the integration domain.†

A further advantage of the localized disturbance generation in the spanwise direction is the additional possibility of studying the spreading of the transition process in the spanwise direction. It was found in simulations that it makes a difference whether the spanwise modulation of the 2-D TS-wave is realized as a steady baseflow deformation or as an unsteady oscillation with the fundamental disturbance frequency. The steady baseflow deformation, as used in Meyer *et al.* (1998), seems to favour a faster spreading of the vortical structures in the spanwise direction. As the current experiment used the unsteady disturbance generation method, we used this method in the DNS as well in order to obtain comparable results.

An omnipresent problem when trying to match the DNS with the experimental results is the sensitivity of the late-stage boundary layer flow to small random background perturbations which are always present under real conditions. It is very difficult to choose the correct initial disturbance amplitudes in the DNS because it is almost impossible to determine whether a given development is caused by a fixed initial amplitude level without additional background perturbations, or by the influence of the background that can lead to a similar development when using a slightly lower amplitude level than in the first case. The random nature of the small-amplitude background makes it very hard to model its influence adequately in the DNS. This uncertainty in the initial conditions leads to a decreasing agreement of the unsteady velocity profiles between experimental and numerical data far downstream in the nonlinear transition process. The exact background spectrum of the DNS is unknown too, because a large number of simulation periods would be needed in order to obtain a converged statistic, which is impractical because of high computational costs. But in general, when no artificial noise is introduced in the simulation, the background noise level is several orders of magnitude less than in the experiment. Despite all these unknowns, the agreement of the averaged profiles achievable is very good over the full range of the transition process, and the development of the dominant unsteady structures is also found to agree very well.

† The main reason for the different spanwise wavenumbers is that some measurements were performed even further downstream than intended for comparison with the DNS. Therefore, the width of the integration domain in the DNS could be chosen smaller without any significant vortical interactions taking place. For comparing the modal behaviour, data from the same spanwise range were analysed in both experiment and DNS.

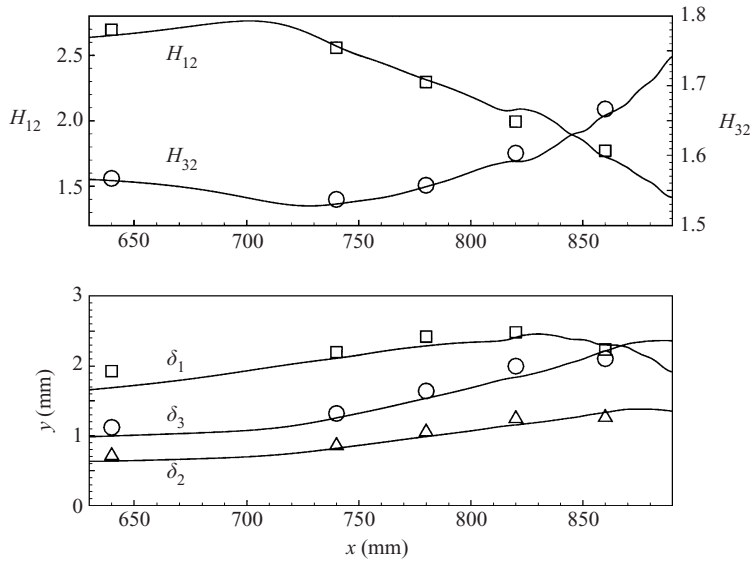

FIGURE 5. Development of the shape factors H_{12} and H_{32}, the boundary-layer displacement thickness δ_1, the momentum thickness δ_2, and the energy loss thickness δ_3, along the centreline $z = 0$ mm in the K-regime. Experiment (symbols) vs. DNS (lines).

The parameters of the simulation are given in table 1. The numerical results have been checked by grid refinement tests with even higher resolution and by comparison with the experimental results. The wall-normal direction turned out to be the critical one in terms of the resolution requirements.

5. Comparison of the results

5.1. *Mean-flow characteristics*

For the undisturbed flow, the mean-velocity profiles in the range of the measurements are very close to the Blasius profile, i.e. the zero-pressure-gradient boundary-layer flow. The experimentally determined shape factor H_{12} is in general lower (max. -3.5%) than the theoretical value $H_{12} = 2.59$ because of the slight favourable pressure gradient due to the boundary-layer growth in the axisymmetric test section. The value of H_{32} is only slightly higher (max. 1.3%) than the theoretical value $H_{32} = 1.57$. The development of the displacement thickness is shown in figure 3.

For the disturbed flow, a deviation of the mean profile from the theoretical Blasius value can already be observed at $x = 740$ mm in the peak plane, i.e. along the centreline of the maximum excitation (see figure 5). The shape factor goes continuously down to a value of $H_{12} = 1.77$ at $x = 860$ mm with a profile displaying an inflection point. The comparison of the experimental results with the DNS data shows very good agreement for the shape-factors and the integrated boundary-layer thicknesses.

For a better quantitative understanding of the transitional flow, normal-to-wall profiles of the mean and fluctuation velocities of the disturbed boundary layer are shown in figure 6. The deformed mean-velocity profiles along the peak plane in experiment and DNS compare well over the whole range of the transition process. In contrast to the peak plane, almost no deformation of the mean-velocity profile can be observed in the valley region at $z = \pm 24$ mm in both the experiment and the DNS (not shown).

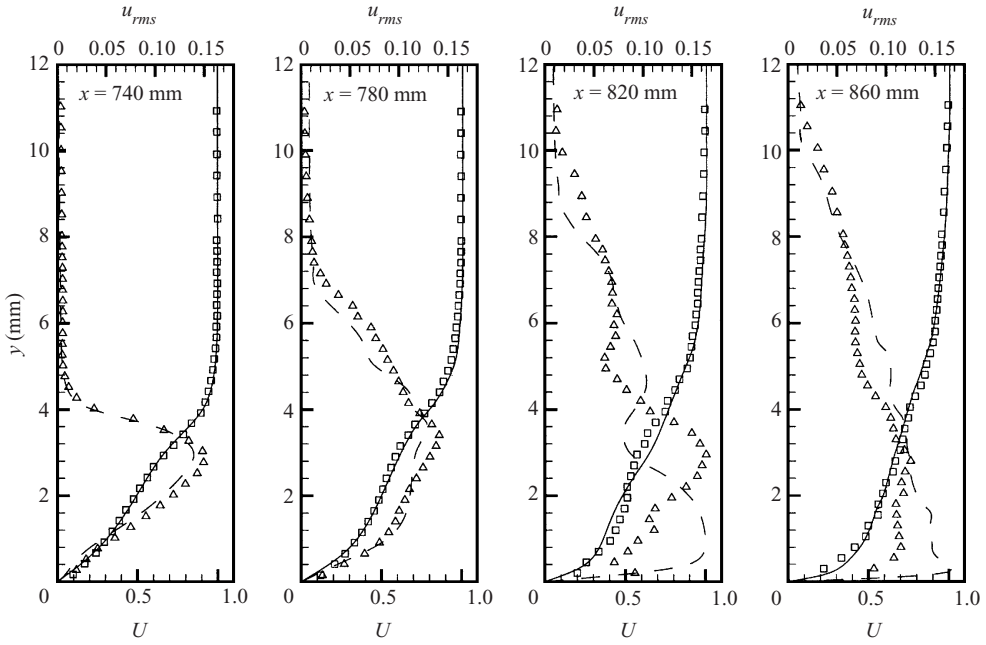

FIGURE 6. Mean velocity (——) and fluctuation (– – –) profiles normalized with U_∞ at $z = 0$ mm and four different x-positions (x = 740, 780, 820, 860 mm). Experiment (△, u_{rms}; □, U) vs. DNS (lines).

5.2. *Disturbance characteristics and structure*

The profile of the fluctuation velocity u' at the first x-position in figure 6 shows a strong maximum near the outer edge of the boundary layer ($u'_{max} = 14\%$). At this position, the first well-developed spike was observed in the velocity time traces. The quantitative agreement of the fluctuation velocity profiles between DNS and experiment is decreasing with increasing x-position, but the qualitative shape remains similar. The reasons for this increasing deviation have already been discussed in § 4.

A comparison between experiment and DNS at four x-positions in (y, z, t) spaces is shown in figure 7. It documents the development of the velocity disturbances in the K-regime. Plotted are iso-surfaces of the periodic streamwise velocity fluctuation u'_p for two fundamental periods in time. Dark iso-surfaces represent negative velocity fluctuations (−8%), whereas light iso-surfaces represent positive velocity fluctuations (+8%). The disturbance structures develop almost identically in the experiment and in the simulation. Starting from a Λ-shape inclined to the wall, the development of secondary side structures and spikes can be observed. The dark spots at the tip of the structures correspond to strong negative velocity fluctuations, i.e. the spikes in the time traces. The number and position of the spikes agree well. Possible reasons for the slightly decreasing agreement at further downstream positions were already discussed in § 4.

The results from a computation of the frequency–wavenumber spectra, as described in § 2, are shown in figure 8. Plotted are the maxima of the modes in the wall-normal profile, lines for the simulation and symbols for the experiment. The disturbance generation of the DNS is adjusted to match the spanwise and wall-normal distribution of the amplitude of the fundamental frequency found in the experiment at the first measurement position (x = 640 mm) as closely as possible. As a result, the fundamental modes in figure 8 coincide very well. Additionally, the stationary modes,

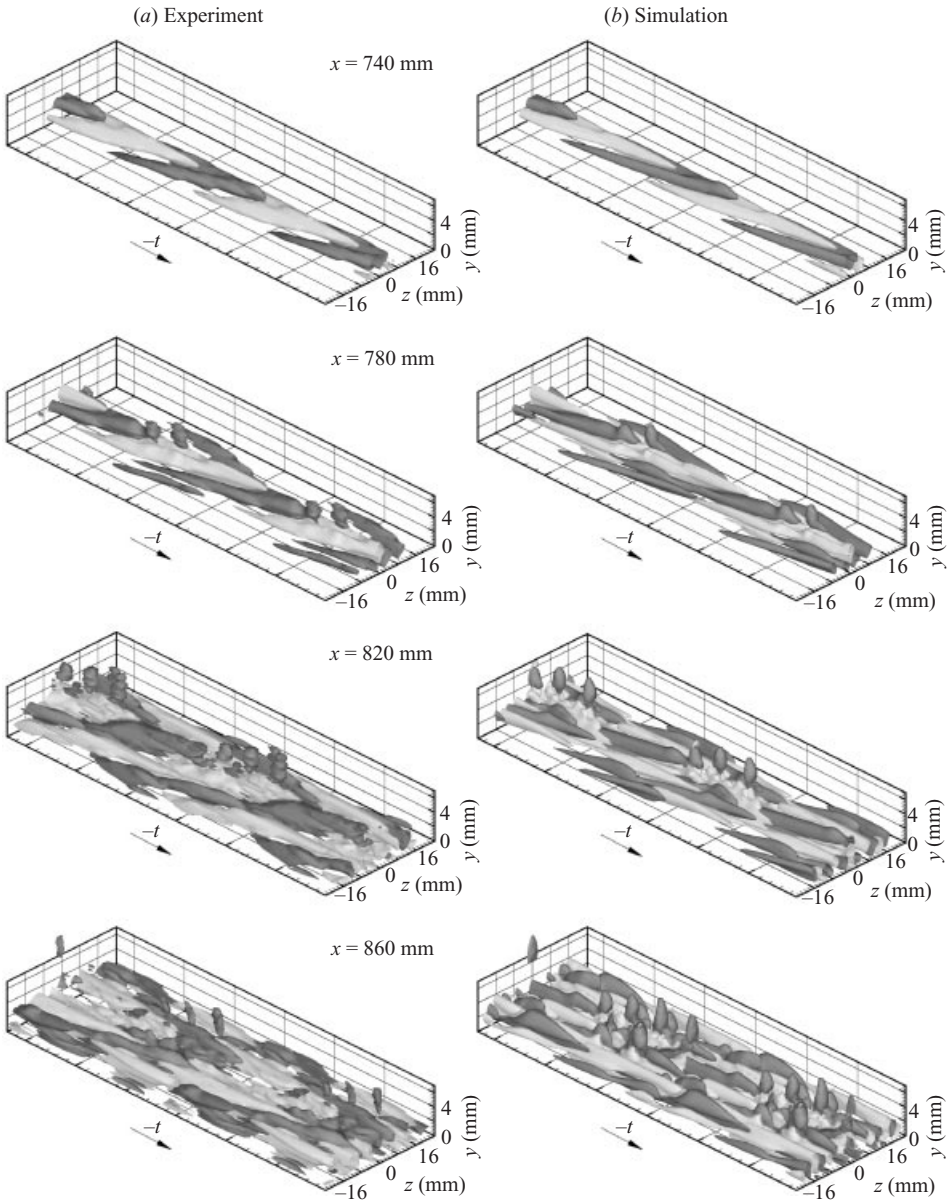

FIGURE 7. Iso-surfaces of the streamwise velocity fluctuation u'_p (light: +8%, dark: −8%) at four consecutive x-positions (x = 740, 780, 820, 860 mm). (*a*) Experiment vs. (*b*) DNS.

as well as the higher harmonic modes, show a good quantitative agreement in their development, despite the very strong nonlinear flow evolution. In figure 8, only waves with very high amplitudes are shown. The complete spectrum contains, of course, a lot more waves. They are generated by the input of a high-amplitude two-dimensional wave plus a number of oblique waves. Additionally, the strong nonlinearities, occurring from the very beginning of the flow development right at the disturbance strip, lead to a rapid filling of the frequency–wavenumber spectrum.

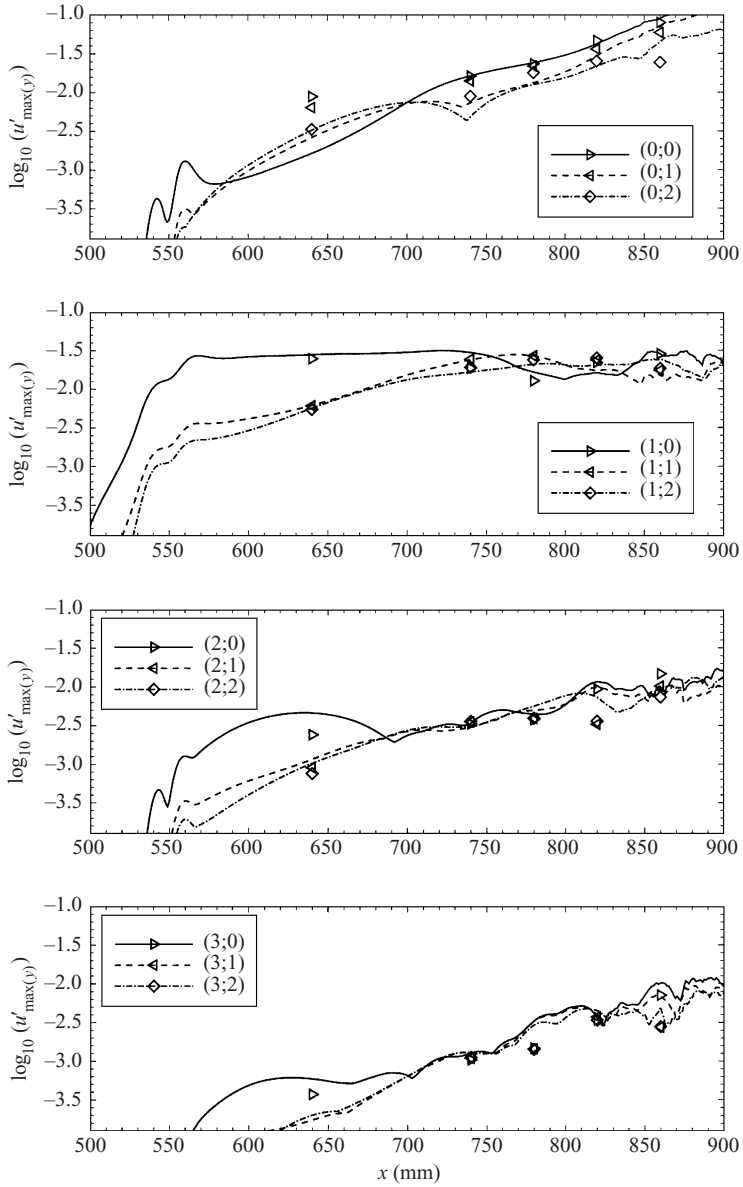

FIGURE 8. Development of the wall-normal maxima of the modes (h;k) in the frequency–wavenumber spectrum, with h being the frequency index and k the spanwise wavenumber index. Experiment (symbols) vs. DNS (lines).

6. Turbulence development

Up to this point we have shown that the agreement between experiment and DNS for the current transitional boundary layer flow is very good. Now we will use the data to gain insight into the mechanism of flow randomization. Since turbulent flow is by definition connected with random fluctuations with respect to the time-averaged flow, the question arises of where these random fluctuations occur first in the otherwise periodically disturbed flow, and how they are amplified. Obviously,

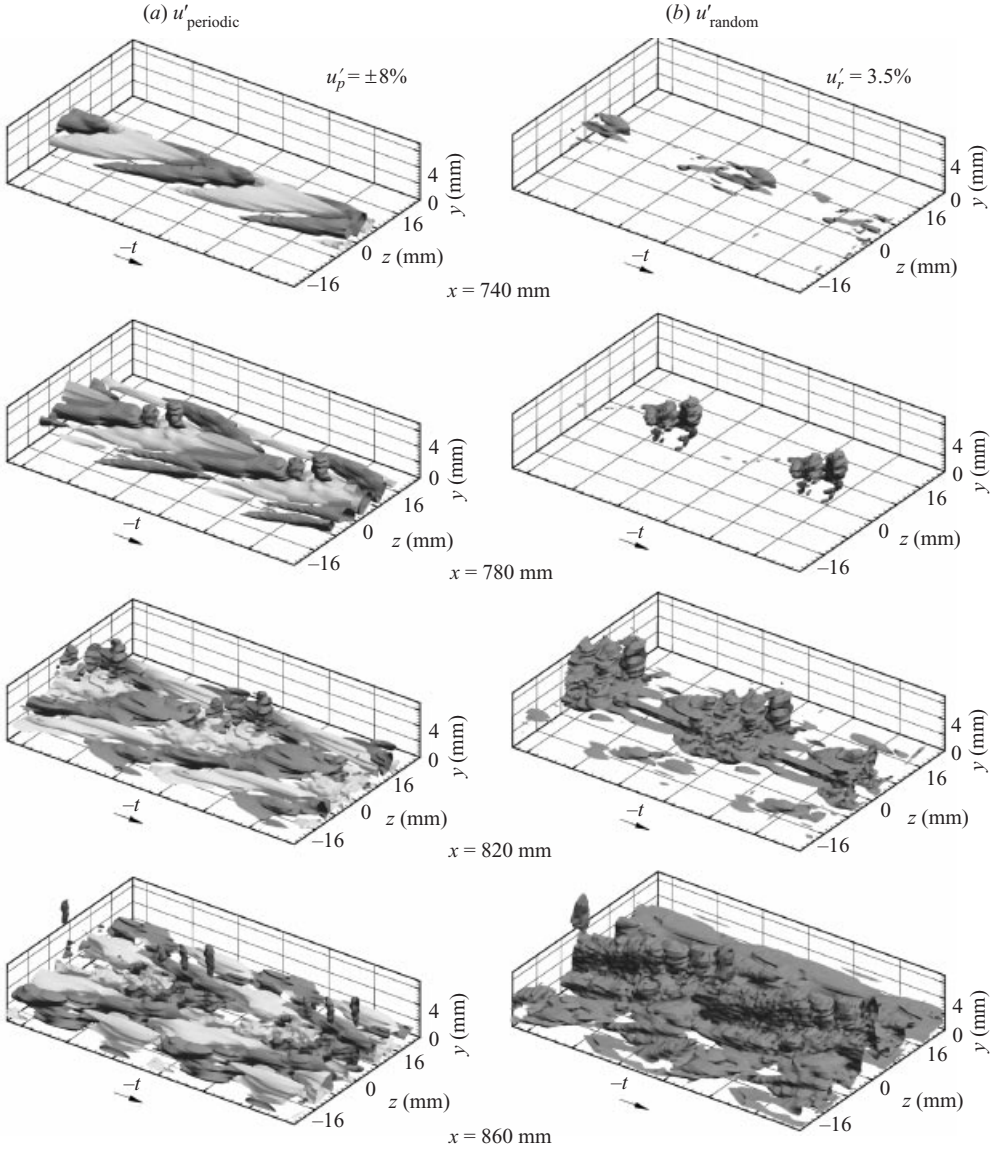

FIGURE 9. Iso-surfaces of two values of the periodic fluctuations $u'_p = \pm 8\%$ (*a*) colour coding as in figure 7) and the r.m.s.-values of the random fluctuations $u'_r = 3.5\%$ (*b*) at four different x-positions ($x = 740$, 780, 820, 860 mm, experimental data).

there must be a connection between the instability mechanisms inherent in the flow and the – in real flow situations always present – small-amplitude random background disturbances. In the following section we try to shed some light on the development of these initial random perturbations which finally lead to a fully turbulent flow. We do not claim to explain the generation of the turbulent flow itself but only the amplification mechanism of the initial random fluctuations in the complex, unsteady and three-dimensional transitional flow.

6.1. *Turbulence development in periodic Λ-structures*

In figure 9, experimental data are used to show the development of the periodic fluctuations u'_p side by side with r.m.s.-values of the random perturbations u'_r. Upstream of the first x-position shown here, no significant random perturbations can be observed, and the flow is purely periodic. The first measurable sign of randomness can be observed at a position corresponding to the tip of the Λ-shaped disturbance structure at $x = 740\,\mathrm{mm}$. At the second x-position, two distinguishable spots of randomness appear at the same location as the dark spots of negative velocity fluctuation, i.e. the spikes in the velocity time traces. The first random velocity fluctuations are identified as phase jitter and amplitude modulations of the ring-like vortex structures at the tip of the Λ-structure in the outer part of the boundary layer. The phase jitter and amplitude modulations can be seen in all non-averaged time traces of periodic transition. From period to period there are visible differences in the amplitude of the spike events and in their temporal separation in the outer part of the boundary layer. Differing temporal separations of the spike events in an initially periodic scenario correspond to a slight spatial displacement of the ring-like vortices which generate the spike signals (see e.g. the time traces in Bake *et al.* 2000, figure 15). At the third and fourth x-positions (multiple spikes) in figure 9, a rapid filling of the flow field with random fluctuations towards the wall, and then in spanwise direction, can be observed. The early randomization is very localized in space and time, and spreads from the region of the spikes to the surrounding fluid and to the wall. When plotting the random fluctuations from DNS data, the amplitude level at which these fluctuations occur is much lower (about two orders of magnitude in a simulation without introducing additional background noise), and the transition process, as measured by the downstream development of the shape factors, is somewhat delayed compared to the experiment. Nevertheless, the non-periodic fluctuations occur at the same locations within the boundary layer in DNS and experiment. When an additional very low-amplitude random background is introduced in the simulation, e.g. by random suction and blowing with very low amplitude at the disturbance strip, the non-periodic fluctuations in the DNS reach the level of the experiment, and only then is the transition process as fast as observed in the experiment.

A cut through the experimental data of figure 9 in the peak plane at $z = 0\,\mathrm{mm}$ is shown in figure 10. Here, the random fluctuations u'_r are plotted in grey scale together with positive values of the periodic part of the wall-normal velocity gradient $\partial U/\partial y$ plotted as contour lines. In boundary layers this gradient is almost equal to the spanwise vorticity Ω_z since $\partial V/\partial x$ is not contributing much (see e.g. Rist & Fasel 1995). The figure illustrates the relative position of the non-periodic fluctuations (grey shades) and the high-shear layers (contour lines) that occur as satellites of the dominant vortical structures in the boundary layer. At first, the strongest random fluctuations can again be observed at the position of the spikes close to the kink of the inclined high-shear layer which coincides with the tip of the Λ-vortex in the outer part of the boundary layer. At only a short distance downstream non-periodic motions also occur close to the wall in the region of strong mean velocity gradients where they are strongly amplified in the following development. The flow structures in (y, t)-space in figure 10 which show the breakdown of a high-shear layer are similar to the ones shown in Lu & Smith (1991) where the bursting phenomenon in turbulent boundary layers was investigated. The structures in that paper were not as organized as in the controlled transition process studied here, but nevertheless the local generation of turbulence in the presence of strong velocity gradients near the wall might be of a similar nature.

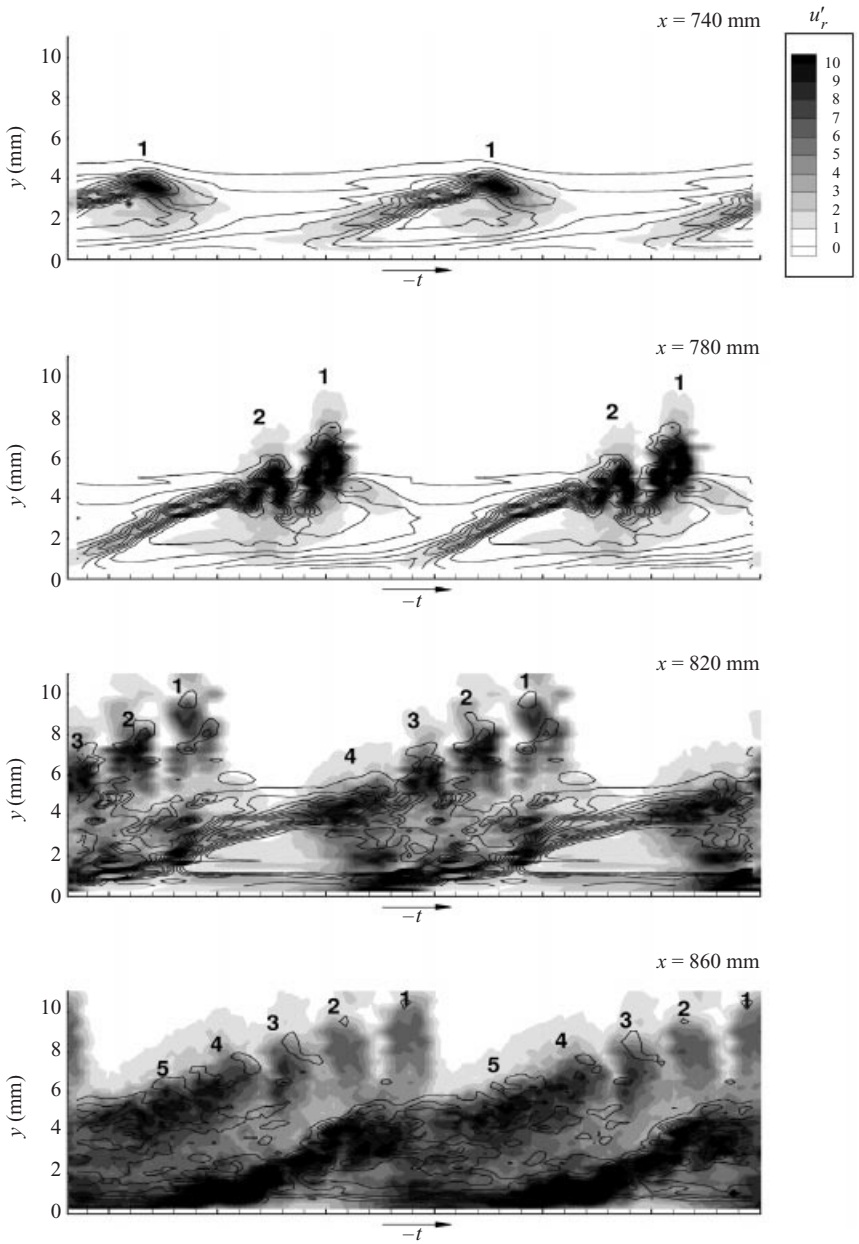

FIGURE 10. Root-mean-square-values of the random streamwise velocity fluctuation u'_r (grey scale) and the periodic part of the wall-normal total velocity gradient $\partial U/\partial y$ (with $U = \bar{u} + u'_p$; contour lines: min = 500 s^{-1}, max = 4500 s^{-1}, step = 500 s^{-1}) at different x-positions. The numbers label the regions of spikes (experimental data).

The flow randomization process can be understood by taking into account the development of the vortical structures in the transitional boundary layer. A vortex identification method introduced by Jeong & Hussain (1995) is applied, which finds vortex cores by locating the inflection points of the pressure in a plane perpendicular to the vortex axis. The pressure inflection points surround the pressure minimum that

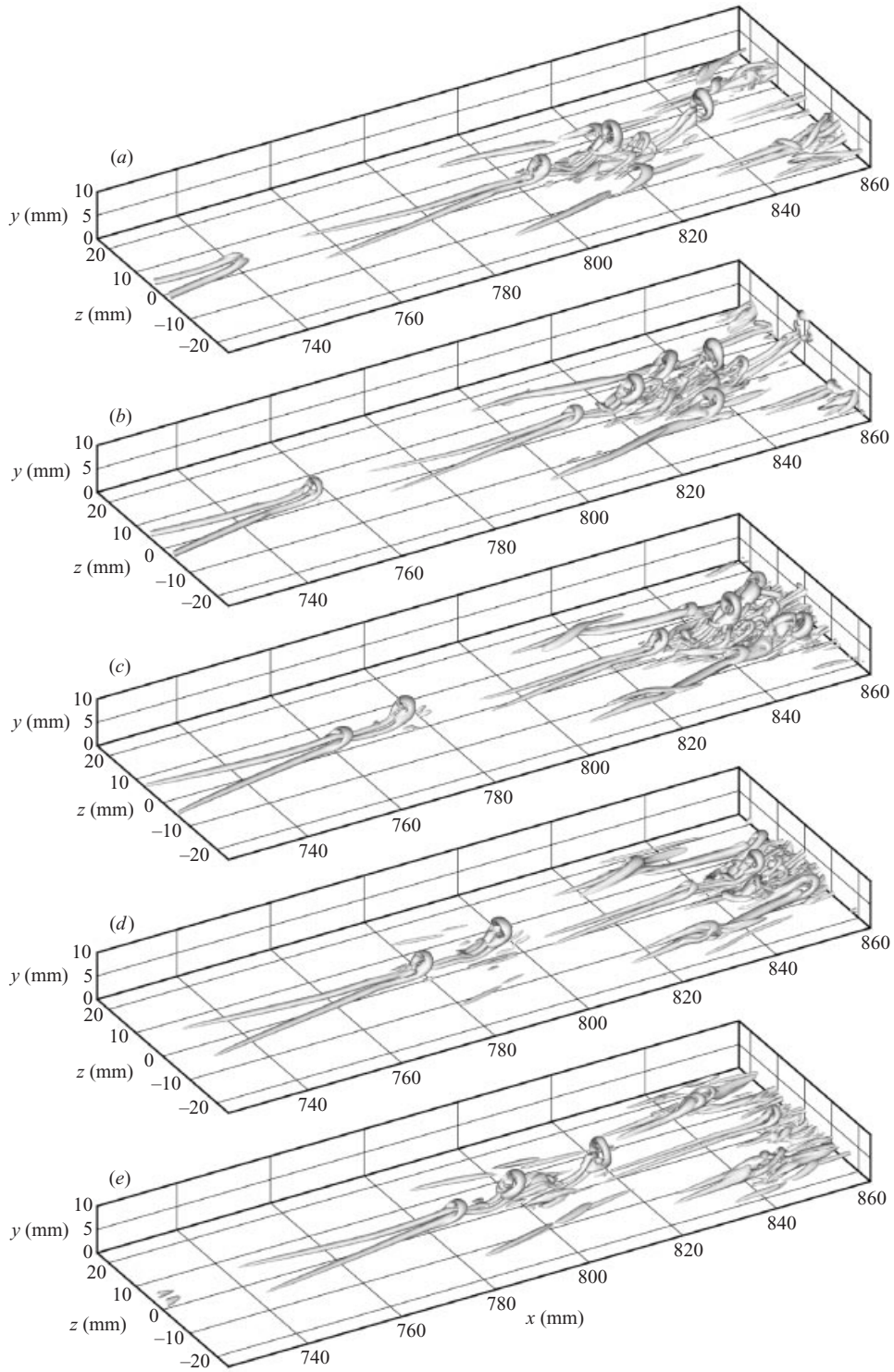

FIGURE 11. Vortex visualization using instantaneous data from the DNS at five time moments within one disturbance period T: (*a*) $t = 0.2T$; (*b*) $t = 0.4T$; (*c*) $t = 0.6T$; (*d*) $t = 0.8T$; (*e*) $t = T$. Iso-level $\lambda_2 = -150$.

occurs in the vicinity of the vortex core. The method is used for the visualization of the development of the coherent vortical motion as shown in figure 11. The data for figure 11 are taken from the DNS, and show the development of the Ω- or ring-like vortices at the tip of Λ-structures together with the formation of secondary structures at positions further away from the peak plane ($z = 0$ mm) at five instants in a fundamental period. Many symmetric, as well as asymmetric, structures develop during the late transition process. At the tip of the Λ-vortex (figure 11*a*, $x \approx 730$ mm), we find a strong upward movement of fluid between the legs of the vortex due to induction by their counter-rotation. This transport of low-speed fluid away from the wall generates a high-shear layer above the legs of the vortex. At the end of the Λ-vortex between its legs (figure 11*d*, $x \approx 740$ mm), we find a rather weak movement of fluid towards the wall that slightly increases the wall shear stress. The high-shear layer generated by the vortical structure is located on top of the Λ-structure at its tip upstream of the latest loop and merges with the wall shear layer at its end.

From figure 11(*c*) the Λ-structure can be seen at two different stages of its development. From $x = 720$ mm to $x = 755$ mm we find the typical Λ-shape of the legs of the vortex, close together at the tip and wider apart at the tail. When looking at the structure generated one period earlier (from $x = 790$ mm to $x = 825$ mm) we see that the legs are now almost parallel. The length of the structure from tip (first ring-like vortex) to tail is basically unchanged (≈ 35 mm). In order to see what consequences this has for the high-shear layer generated by the vortex we should compare figure 11(*c*) with figure 12(*c*). Figure 12 shows cuts through the high-shear layers, represented by the vorticity component Ω_z, in the peak plane ($z = 0$ mm) at time moments corresponding to the ones shown in figure 11. In figure 12(*c*) the region of very high shear for the first Λ-vortex lies approximately in the range $745\text{ mm} < x < 760\text{ mm}$, whereas for the Λ-vortex generated one period earlier the high-shear layer (HSL) lies in the range $795\text{ mm} < x < 825\text{ mm}$, i.e. the latter HSL is about twice as long as the first one. The growth of the shear layer can easily be explained when we recognize that the HSL is a consequence of the presence of the Λ-vortex in the boundary layer. The HSL is produced by the induction effect of the rotating legs of the Λ-vortex. The legs transfer low-speed fluid away from the wall on the inner side of the Λ-vortex and high-speed fluid towards the wall on the outer side of the Λ-vortex. The effectiveness of momentum transport by fluid induction is restricted to a rather short range, thus the high shear is generated only in the direct vicinity of the rotating legs. Consequently, the strongest shear is generated when the rotating legs are very close together, because then the induction of both legs is superposed. The close-to-wall HSL generated at the tail of the Λ-vortex will play a role at the final breakdown process when the structures generated in different periods start to interact.

In figure 11, we can observe ring-like vortices which evolve continuously at the tip of the Λ-structures. Despite the durability of the ring-like vortices in the outer part of the boundary layer, their initial formation seems to be very sensitive to small perturbations, and their streamwise separation with respect to each other varies slightly from period to period. The 'bridges' that are generated between the legs of the Λ-vortex, out of which the ring-like vortices emerge, must be created by a viscous process because vortex lines are reconnected at this stage of the development which cannot be explained by a purely inviscid mechanism. The subsequent detachment of the vortex loops from the tip of the Λ-vortex is a predominantly inviscid process, basically due to self-induction of the deformed vortex line moving in the mean shear, as suggested in the work of Moin *et al.* (1986). We do not think that the HSL

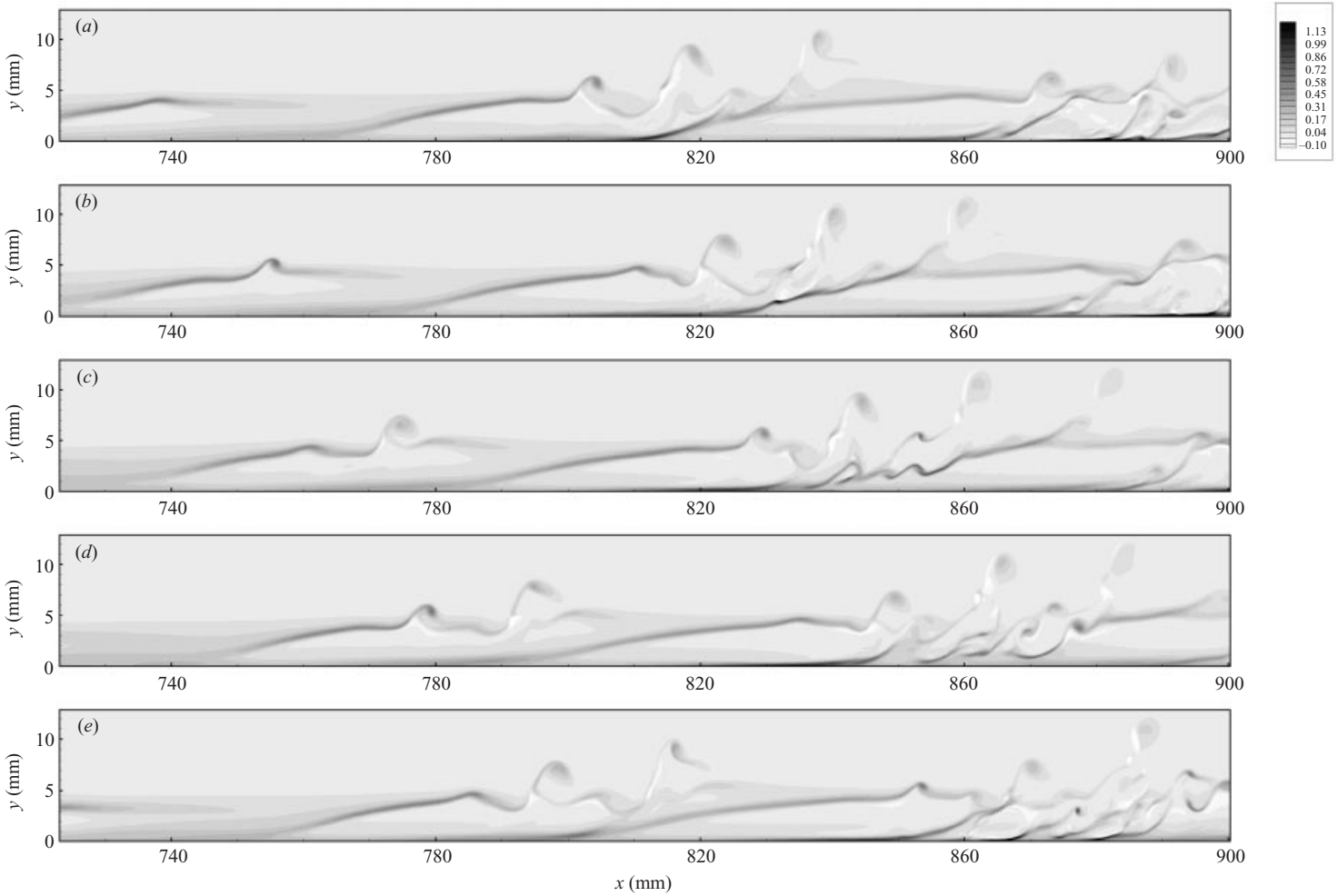

FIGURE 12. Total spanwise vorticity Ω_z in the peak-plane at $z = 0\,\text{mm}$ and at five time moments corresponding to figure 11 (DNS data).

on top of the Λ-vortex simply rolls up into the hairpin vortex (implying that any random disturbances amplified by the HSL will be transfered to ring-like vortices). This concept is based on the observation that the HSL usually ends at the newest ring that is developing at the tip of the Λ-vortex (as it can be observed when looking at the plot of the spanwise vorticity component in figure 12). Between any two ring-like vortices that were originally generated at the tip of the Λ-vortex and already have left the tip, there is only a relatively weak shear layer visible. But this is not necessarily due to the fact that the HSL 'rolls up' into the currently developing ring and therefore disappears, but rather we observe that it starts to disappear (or becomes extremely weak) at the same moment when the strongly rotating legs which connect the two latest vortex loops start moving towards the wall. Instead of pumping low-speed fluid into a region of predominantly high-speed fluid, which would generate a HSL, they propel themselves towards the wall. A strong shear layer is only generated by the swirling motion of a fluid vortex if the rotating vortex is not moving in a direction normal to the axis of the vortex. Here, this would mean that the vortex must stay at about a constant height in the boundary layer in order to generate a HSL (as is the case at the tip of the Λ-vortex but not for the legs connecting the different rings). In our opinion the HSL on top of the Λ-vortex does not disappear because it transforms into a ring-like vortex but rather because it is no longer generated by the vortical motion downstream of the tip of the Λ-vortex. The HSL disappears as soon as the legs connecting the ring-like vortex with the tip of the Λ-vortex start moving towards the wall. We want to point out that the nonlinear breakdown process to turbulence is not caused by a mere inflectional instability of the HSL on top of the Λ-vortex, even if the shear layer visualization in figure 12 might suggest this, but is a much more complicated process involving several different mechanisms. The initial HSL located on top of the Λ-vortex does not seem to be the most important structure for the flow randomization process as we will try to show below.

Our detailed knowledge about the mechanisms which generate the side structures visible in figure 11 is still limited, but possible explanations are discussed in Smith *et al.* (1991) and Smith & Walker (1997) where the generation, development and interaction of hairpin vortices in a turbulent boundary layer was studied. The processes of vortex generation and interaction occurring there are very similar to the ones studied here. Another investigation concerned with the turbulence production mechanism by hairpin vortices was performed by Asai & Nishioka (1995). The authors suggested an inflectional instability of the 3-D wall shear layer lifted up by the longitudinal vortex legs as a possible explanation for the growth of the near-wall vortical structures.

Downstream of $x \approx 820$ mm, we found the typical turbulent velocity profile normalized in wall coordinates with a buffer region, a log layer and a wake region, but still with a considerable dependence of the friction velocity on the downstream and spanwise position (not shown here). Visual inspection of figure 11 seems to support the findings reported by Robinson (1991) that the buffer region very close to the wall is dominated by quasi-streamwise vortices which generate the typical low- and high-speed streaks appearing later in the fully turbulent boundary layer, whereas the wake region in the outer part of the boundary layer is dominated by transverse vortices and vortical arches (mainly the ring-like vortices in the flow studied here). The log region in between is dominated by the presence of both types of organized vortical structures, streamwise as well as transverse.

The flow randomization process can be summarized as follows:

(*a*) The first random fluctuations are observed in the experiment at the tip of the Λ-vortex, where the ring-like vortices are formed. They, in turn, generate the spike

signals in the time traces by induction. This formation process is very sensitive to background perturbations, as mentioned by Borodulin *et al.* (1999), and also observed in turbulent channel flow by Zhou *et al.* (1999). The exact reason why the formation is sensitive to background perturbations still needs further investigation. Possible options are: (i) an instability of the almost parallel vortices at the tip of the Λ-vortex (Crow instability), (ii) an influence of the HSL on top of the Λ-vortex (strong local velocity gradients close to the reconnection region) or (iii) a sensitivity of the inviscid self-induction process to small disturbances. The reconnection process is accompanied by strong vortex stretching when the developing Ω-vortex lifts up in the boundary layer and is therefore accelerated. The stretching leads to increased fluid induction, and, therefore, to a region of extremely high shear slightly above the stretched vortex legs. This shear layer disappears when the Ω-vortex detaches from the tip of the Λ-vortex and the legs still connecting it with the tip of the Λ start moving towards the wall. The sensitivity of the process of formation of the ring-like vortices to small random background perturbations is responsible for a slightly varying occurrence of the ring-like vortices in space and time from one period to another. These variations are perceived in the experiment as phase jitter and small-amplitude variations of the spike signals, as already discussed at the beginning of § 6.1. Since the fluid region around the ring-like vortices is a region of strong local velocity gradients, the small-amplitude background perturbations will be amplified at these locations. Therefore, the amplified random motions will still be connected to the periodically occurring events in the flow, i.e. they will be strongest in regions where the local flow structures generate the largest gradients; they are no longer completely independent background perturbations. Related investigations were performed by Nishioka (1994) for the case of plane Poiseuille flow. He investigated the influence of the background perturbations on the flow randomization process through the secondary instability. It was found that the non-periodic motions which are represented by the continuous part of the spectrum are connected with the periodic events in the boundary layer and are not completely random fluctuations.

(*b*) Once formed, the ring-like vortices have a strong effect on the surrounding fluid, especially down to the region close to the wall as already presented by Meyer *et al.* (1999). Positive velocity fluctuations are observed in a plane $z \approx \pm 2\,\mathrm{mm}$ that move with the same speed as the ring-like vortices but are much closer to the wall. This influence can also be clearly observed in animations of $\partial U/\partial y$ at the wall produced from DNS data. The modulation patterns of the wall values can be clearly attributed to the ring-like vortices in the outer part of the boundary layer. They move with the same velocity as the ring-like vortices themselves, which is almost the free-stream speed. This way, the random motion in the outer part of the boundary layer has an influence on the region close to the wall where strong mean velocity gradients occur and the non-periodic fluctuations are amplified. For this amplification, one mechanism was proposed by Dryganets *et al.* (1990). They found a detuned subharmonic-type resonant interaction responsible for the amplification of random disturbances in the presence of a deterministic fundamental wave.

(*c*) A mechanism different from induction that partly explains the effect that the coherent structures in the outer part of the boundary layer have on the region close the wall becomes obvious when we consider the instantaneous pressure field generated by the Λ-vortex in the boundary layer. In figure 13, cuts through the pressure field in the plane $z = 0\,\mathrm{mm}$ and at the wall are shown at a stage where the Λ-vortex has two fully developed Ω-vortices at its tip. Due to the low-pressure regions present within the vortex core, and at the locations where very strong induction occurs, pressure

gradients are also generated at the wall. According to Lighthill (1963), pressure gradients along the wall will influence the production process of new vorticity at the wall. Therefore, the evolution of the coherent structures in the outer part of the boundary layer will directly influence the vorticity production at the wall. The pressure gradients may not be as pronounced in the ensuing turbulent boundary layer because of the huge number of structures in the flow, but for this stage of the flow development they seem to be relevant.

(*d*) Further downstream, the amplification process of background disturbances becomes even more complex when the vortical structures and high-shear layers generated in different disturbance periods start to interact. Starting at about $x = 800$ mm in figure 12(*d*), the ring-like vortices of a given disturbance period catch up with the structures generated one period before. The interaction of the ring-like vortices with the high-shear layer generated by the tail of the preceding Λ-vortex close to the wall, and with its legs, generates very strong shear that moves very quickly towards the wall ($x \approx 810$ mm in figure 12*a*). As an additional effect, the legs that connect the accelerated ring-like vortices with the tip of the Λ-vortex, or with the ring next to them, are strongly stretched and propel themselves towards the wall where the already existing high-shear layer is intensified (compare $x \approx 810$ mm in figures 11*a* and 12*a*). Many new small vortical structures and high-shear layers come into existence in the following development through these interactions, which can be easily observed comparing figures 11 and 12. This conglomeration of new structures might itself be very sensitive to background disturbances because of the complex interactions that occur between them. Most likely, the non-periodic motion from the upstream development as described in (*a*)–(*c*) above will be amplified and spread to the sides of the peak plane in this environment.

This picture of the randomization process seems to be confirmed by the experimental data in figure 10. The inclined high-shear layer between the legs of the Λ-vortex breaks down (increasing randomization) starting first at the tip of the Λ-vortex, and, only shortly later, in the wall region, too. In this process, the strongest $\partial U/\partial y$ occurs below the spikes close to the wall and not in the high-shear layer that appears as a satellite on top of and between the Λ-vortex legs – the difference of the $\partial U/\partial y$ shown here to Ω_z as plotted in figure 12 from DNS data is only of the order of 10%. Eventually, the regions of strong random velocity fluctuations in the layer closest to the wall enlarge and merge. The near-wall peak in the u'_{rms} profile typical of a turbulent boundary layer is developing (see figure 6, $x = 860$ mm) and finally the shape factor H_{12} approaches a value of about 1.54 (see figure 5). The turbulent value of $H_{12} \approx 1.4$ will finally be reached further downstream.

Nishioka (1994) has investigated the influence of non-periodic background disturbances (i.e. disturbances that are part of the continuous spectrum) in spectral space. These results show a selection of background disturbances which have a certain phase relation to the fundamental disturbance and its higher harmonics. As a consequence, this leads to a coupling of the continuous-spectrum modes with the formation of the spikes and the high-shear layer. Amplification of these disturbances by a high-frequency instability of the high-shear layer will then lead to a breakdown into hairpin vortices. In the present paper we have tried to show that the breakdown process of the Λ-structure and the flow randomization process is somewhat more complicated than a mere inflectional shear-layer instability to high-frequency disturbances. Nevertheless, this spectral point of view of the breakdown process is complementary to the structure-based view of the breakdown process as presented in the present paper. Since it is clear that all Fourier modes that are

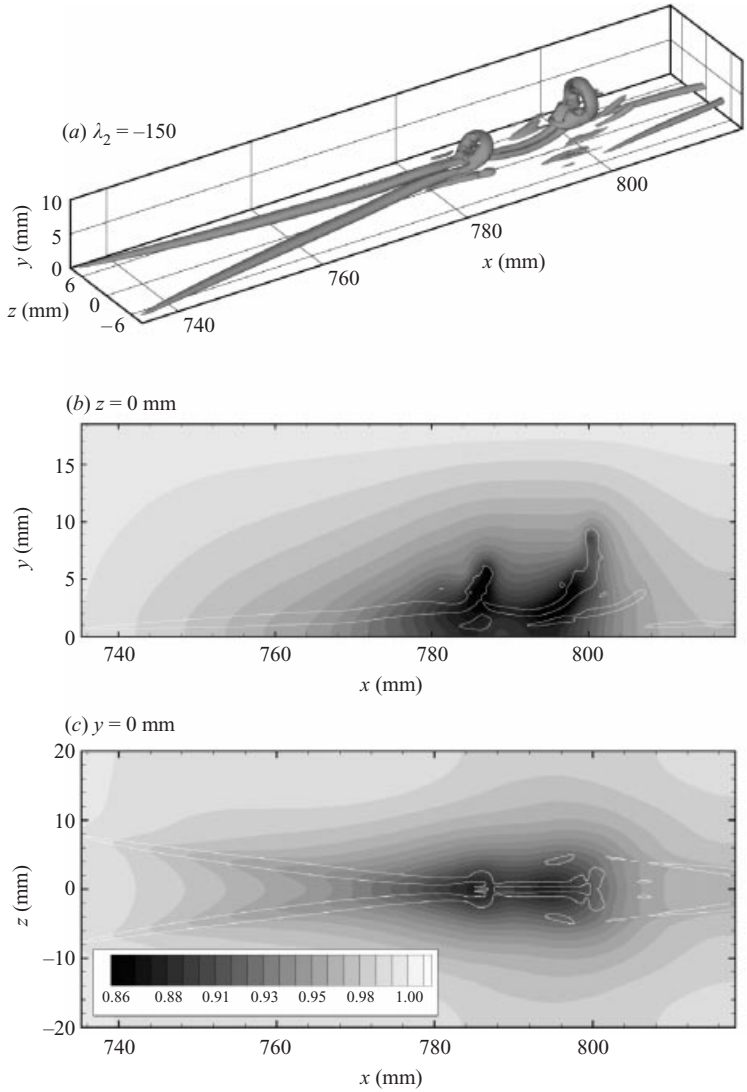

FIGURE 13. (*a*) Vortex visualization from DNS data and (*b*, *c*) cuts through the instantaneous pressure field. The undisturbed pressure level is 1.0 as $y \rightarrow \infty$. The pressure field is dominated by the presence of the vortical structure. Pressure gradients along the wall are generated that will influence the vorticity production at the wall.

needed to represent a certain structure in space and time must be correlated, these earlier findings are consistent with the present observations in that respect. From our viewpoint the phase-coupled background disturbances manifest themselves as displacements of flow structures with respect to each other from event to event (compared to the periodic case). In addition to that, we can observe now that these effects are not confined to the high-shear layer near the outer edge of the boundary layer, but influence the shear near the wall in an unsteady manner. Apparently this is the next step towards turbulence after the formation of hairpin (or Ω-) eddies.

7. Conclusions

In the experiment, the flow field was analysed with the help of phase-locked ensemble-averaged hot-wire measurements. The spatial formation of the disturbance structures in the Klebanoff-type transition was followed up to the development of turbulence. The experimental results are compared with the results of a DNS. The disturbance spectrum of the DNS was adjusted to match the disturbance spectrum of the experiment as closely as possible. Good agreement was found for the development of the normal oblique modes and the topological evolution of the vortex structures. The DNS data are used to identify vortex structures and their interaction in order to explain the amplification of non-periodic motions in the transition process that leads from laminar to turbulent flow.

The first sign of randomness in the transition process was observed at a position corresponding to the tip of the Λ-vortex – a Λ-shaped disturbance structure that typically appears in the transition process studied here. At this position, a ring-like vortex structure that induces the spike signals in the velocity time traces is formed at slightly different positions from period to period because of the small random background perturbations always present under real conditions. These random fluctuations can be identified as phase jitter and amplitude modulations of the spike signals in measurements. The ring-like vortices strongly influence the near-wall structures by induction and by generating pressure gradients along the wall. Thus, the initial non-periodic motion of the ring-like vortices in the outer part of the boundary layer initiates random fluctuations near the wall which are then strongly amplified close to the wall where strong mean velocity gradients prevail. The mechanism of vortex stretching of the 'legs' of the ring-like vortices, their motion towards the wall, and their interaction with vortices of the Λ-structure generated one period earlier, intensifies the formation of a very strong, near-wall high-shear layer below the spikes that quickly breaks down due to the interaction with the structures above in the outer part of the boundary layer. At further downstream positions, a rapid filling of the flow field with random fluctuations towards the wall, and then in the spanwise direction, was observed that finally leads to a quasi-random turbulent flow. The amplification of the random disturbances is always connected with the large local velocity gradients generated by the coherent motion within the boundary layer, and with the complex interaction of the countless structures generated continuously during the transition process.

The authors are grateful for the helpful advice from Professor H.-H. Fernholz and Professor Y. S. Kachanov. The projects were supported by the Deutsche Forschungs-Gemeinschaft (DFG) within the 'Schwerpunktprogramm Transition'. Computer time on Cray-T3E/512 and NEC-SX/5 was provided by Höchstleistungsrechenzentrum Stuttgart (HLRS).

REFERENCES

Acalar, M. S. & Smith, C. R. 1987*a* A study of hairpin vortices in a laminar boundary layer. Part 1. Hairpin vortices generated by a hemisphere protuberance. *J. Fluid Mech.* **175**, 1–41.

Acalar, M. S. & Smith, C. R. 1987*b* A study of hairpin vortices in a laminar boundary layer. Part 2. Hairpin vortices generated by fluid injection. *J. Fluid Mech.* **175**, 43–83.

Asai, M. & Nishioka, M. 1995 Boundary-layer transition triggered by hairpin eddies at subcritical Reynolds numbers. *J. Fluid Mech.* **297**, 101–122.

Bake, S., Fernholz, H. H. & Kachanov, Y. S. 2000 Resemblance of K- and N-regimes of boundary-layer transition at late stages. *Eur. J. Mech.* B/*Fluids* **19**, 1–22.

Berlin, S., Wiegel, M. & Henningson, D. S. 1999 Numerical and experimental investigation of oblique boundary layer transition. *J. Fluid Mech.* **393**, 23–57.

Borodulin, V. I., Gaponenko, V. R., Kachanov, Y. S., Lian, Q. X., Qin, Y. H., Guo, H. & Lee, C. B. 1999 Experimental study of mechanisms of flow randomization at late stages of boundary layer transition. In *Intl Symp. on Actual Problems of Physical Hydroaerodynamics, Trans. Part II*, pp. 25–26. Novosibirsk: Inst. Thermophysics.

Borodulin, V. I. & Kachanov, Y. S. 1989 The role of the mechanism of the local secondary instability in K-breakdown of boundary layer. *Sov. J. Appl. Phys* **3** (2), 70–81.

Borodulin, V. I. & Kachanov, Y. S. 1995 Formation and development of coherent structures in a transitional boundary layer. *J. Appl. Mech. Tech. Phys.* **36** (4), 60–97.

Dryganets, S. V., Kachanov, Y. S., Levchenko, V. Y. & Ramanzanov, M. P. 1990 Resonant flow randomization in the K-regime of boundary layer transition. *J. Appl. Mech. Tech. Phys.* **2**, 83–94 (transl. *J. Appl. Mech. Tech. Phys.* 1990, **31**, 239–249).

Falco, R. E. 1977 Coherent motions in the outer region of turbulent boundary layers. *Phys. Fluids,* **20**, S124–S132.

Fasel, H. F., Rist, U. & Konzelmann, U. 1990 Numerical investigation of the three-dimensional development in boundary-layer transition. *AIAA J.* **28**, 29–37.

Fernholz, H. H. & Warnack, D. 1998 The effect of a favourable pressure gradient and of the Reynolds number on an incompressible axisymmetric turbulent boundary layer. Part 1. The turbulent boundary layer. *J. Fluid Mech.* **359**, 329–356.

Gilyov, V. M., Kachanov, Y. S. & Kozlov, V. V. 1983 Development of a spatial wave packet in a boundary layer. *Izv. Sib. Otd. Akad. Nauk SSSR, Ser. Tekh. Nauk.* **13** (3), 27–37 (in Russian).

Haidari, A. H. & Smith, C. R. 1994 The generation and regeneration of single hairpin vortices. *J. Fluid Mech.* **277**, 135–162.

Hama, F. R. 1959 Some transition patterns in axisymmetric boundary layers. *Phys. Fluids* **2**, 664–667.

Hama, F. R. & Nutant, J. 1961 Self-induced velocity on a curved vortex. *Phys. Fluids* **4**, 28–32.

Hama, F. R. & Nutant, J. 1963 Detailed flow-field observations in the transition process in a thick boundary layer. In *Proc. Heat Transfer and Fluid Mech. Inst.*, pp. 77–93. Stanford University Press.

Head, M. R. & Bandyopadhyay, P. R. 1981 New aspects of turbulent boundary-layer structure. *J. Fluid Mech.* **107**, 297–338.

Jeong, J. & Hussain, F. 1995 On the identification of a vortex. *J. Fluid Mech.* **285**, 69–94.

Kachanov, Y. S. 1994 Physical mechanisms of laminar boundary-layer transition. *Annu. Rev. Fluid Mech.* **26**, 411–482.

Kachanov, Y. S. & Michalke, A. 1994 Three-dimensional instability of flat plate boundary layers: Theory and experiment. *Eur. J. Mech.* B/*Fluids* **13**, 401–422.

Klebanoff, P., Tidstrom, K. D. & Sargent, L. M. 1962 The three-dimensional nature of boundary-layer transition. *J. Fluid Mech.* **12**, 1–34.

Kleiser, L. & Zang, T. A. 1991 Numerical simulation of transition in wall-bounded shear flows. *Annu. Rev. Fluid Mech.* **23**, 495–537.

Kloker, M. J. 1998 A robust high-resolution split-type compact FD scheme for spatial direct numerical simulation of boundary-layer transition. *Appl. Sci. Res.* **59**, 353–377.

Kloker, M., Konzelmann, U. & Fasel, H. 1993 Outflow boundary conditions for spatial Navier–Stokes simulations of transition boundary layers. *AIAA J.* **31**, 620–628.

Kovasznay, L. S. G., Komoda, H. & Vasudeva, B. R. 1962 Detailed flow field in transition. In *Proc. Heat Transfer and Fluid Mech. Inst.*, pp. 1–26. Stanford University Press.

Lighthill, M. J. 1963 Introduction. Boundary layer theory. In *Laminar Boundary Layers* (ed. L. Rosenhead), pp. 54–61. Oxford University Press.

Lu, L.-J. & Smith, C. R. 1991 Use of quantitative flow visualization data for examination of spatial-temporal velocity and bursting characteristics in a turbulent boundary layer. *J. Fluid Mech.* **232**, 303–340.

Meyer, D. G. W., Rist, U., Borodulin, V. I., Gaponenko, V. R., Kachanov, Y. S., Lian, Q. X. & Lee, C. B. 1999 Late-stage transitional boundary-layer structures. Direct numerical simulation and experiment. In *IUTAM Symp. on Laminar–Turbulent Transition, Sedona, AZ* (ed. H. Fasel & W. Saric), pp. 167–172. Springer.

Meyer, D. G. W., Rist, U. & Wagner, S. 1998 DNS of the generation of secondary Λ-vortices

in a transitional boundary layer. In *Advances in Turbulence VII* (ed. U. Frisch), pp. 97–100. Springer.

Moin, P., Leonard, A. & Kim, J. 1986 Evolution of a curved vortex filament into a vortex ring. *Phys. Fluids* **29**, 955–963.

Morkovin, M. V. 1969 On the many faces of transition. In *Viscous Drag Reduction* (ed. C. Wells), pp. 1–31. Plenum.

Nishioka, M. 1994 Some fundamental problems on transition to wall turbulence. In *IUTAM Symp. on Laminar–Turbulent Transition, Sendai, Japan* (ed. R. Kobayashi), pp. 15–26. Springer.

Nishioka, M. & Asai, M. 1984 Evolution of Tollmien–Schlichting waves into wall turbulence. In *Turbulence and Chaotic Phenomena in Fluids* (ed. T. Tatsumi), pp. 87–92. North-Holland.

Nishioka, M., Asai, M. & Iida, S. 1980 An experimental investigation of the secondary instability. In *IUTAM Sym. on Laminar–Turbulent Transition* (ed. R. Eppler & H. Fasel), pp. 37–46. Springer.

Nishioka, M., Asai, M. & Iida, S. 1981 Wall phenomena in the final stage of transition to turbulence. In *Transition and Turbulence* (ed. R. Meyer), pp. 113–126. Academic.

Orszag, A. S. 1971 Numerical simulation of incompressible flows within simple boundaries. *Stud. Appl. Maths* **1**, 293–327.

Rist, U. 1990 Numerische Untersuchung der räumlichen, dreidimensionalen Störungsentwicklung beim Grenzschichtumschlag. Dissertation, Inst. A f. Mech. Univ. Stuttgart.

Rist, U. & Fasel, H. 1995 Direct numerical simulation of controlled transition in a flat-plate boundary layer. *J. Fluid Mech.* **298**, 211–248.

Rist, U. & Kachanov, Y. S. 1995 Numerical and experimental investigation of the K-regime of boundary-layer transition. In *Laminar–Turbulent Transition, IUTAM Symp. 1994 Sendai, Japan* (ed. R. Kobayashi), pp. 405–412. Springer.

Robinson, S. K. 1991 Coherent motions in the turbulent boundary layer. *Annu. Rev. Fluid Mech.* **23**, 601–639.

Schubauer, G. B. & Skramstad, H. K. 1947 Laminar boundary-layer oscillations and stability of laminar flows. *J. Aero. Sci.* **14**, 69–78.

Smith, C. R. & Walker, J. D. A. 1997 The role of vortex development and interactions. In *Self-sustaining Mechanisms of Wall Turbulence* (ed. R. L. Panton), pp. 13–47. Wiley.

Smith, C. R., Walker, J. D. A., Haidari, A. H. & Sobrun, U. 1991 On the dynamics of near-wall turbulence. *Phil. Trans. R. Soc. Lond.* A **336**, 131–175.

Theodorsen, A. 1952 The structure of turbulent shear flow. *Proc. 2nd Midwestern Conf. on Fluid Mech.* Ohio State University, Columbus, Ohio.

Wray, A. & Hussaini, M. Y. 1984 Numerical experiments in boundary-layer transition. *Proc. R. Soc. Lond.* A **392**, 373–389.

Zang, T. A. & Hussaini, M. Y. 1987 Numerical simulation of nonlinear interactions in channel and boundary-layer transition. In *Nonlinear Wave Interactions in Fluids* (ed. T. H. R. W. Miksad & T. R. Akylas), pp. 131–145. ASME.

Zhou, J., Adrian, R. J., Balchandar, S. & Kendall, T. M. 1999 Mechanism for generating coherent packets of hairpin vortices in channel flow. *J. Fluid Mech.* **387**, 353–396.